BELLE2-CONF-PH-2020-006
August 11, 2020

Rediscovery of $B \to \phi K^{(*)}$ decays and measurement of the longitudinal polarization fraction f_L in $B \to \phi K^*$ decays using the Summer 2020 Belle II dataset

F. Abudinén,[47] I. Adachi,[24,21] R. Adak,[18] K. Adamczyk,[72] P. Ahlburg,[109] J. K. Ahn,[54] H. Aihara,[127] N. Akopov,[133] A. Aloisio,[97,40] F. Ameli,[44] L. Andricek,[63] N. Anh Ky,[37,14] D. M. Asner,[3] H. Atmacan,[111] V. Aulchenko,[4,74] T. Aushev,[26] V. Aushev,[88] T. Aziz,[89] V. Babu,[12] S. Bacher,[72] S. Baehr,[51] S. Bahinipati,[28] A. M. Bakich,[126] P. Bambade,[106] Sw. Banerjee,[116] S. Bansal,[79] M. Barrett,[24] G. Batignani,[100,43] J. Baudot,[107] A. Beaulieu,[129] J. Becker,[51] P. K. Behera,[31] M. Bender,[59] J. V. Bennett,[120] E. Bernieri,[45] F. U. Bernlochner,[109] M. Bertemes,[34] M. Bessner,[113] S. Bettarini,[100,43] V. Bhardwaj,[27] B. Bhuyan,[29] F. Bianchi,[103,46] T. Bilka,[7] S. Bilokin,[59] D. Biswas,[116] A. Bobrov,[4,74] A. Bondar,[4,74] G. Bonvicini,[131] A. Bozek,[72] M. Bračko,[118,87] P. Branchini,[45] N. Braun,[51] R. A. Briere,[5] T. E. Browder,[113] D. N. Brown,[116] A. Budano,[45] L. Burmistrov,[106] S. Bussino,[102,45] M. Campajola,[97,40] L. Cao,[109] G. Caria,[119] G. Casarosa,[100,43] C. Cecchi,[99,42] D. Červenkov,[7] M.-C. Chang,[17] P. Chang,[70] R. Cheaib,[110] V. Chekelian,[62] Y. Q. Chen,[123] Y.-T. Chen,[70] B. G. Cheon,[23] K. Chilikin,[57] K. Chirapatpimol,[8] H.-E. Cho,[23] K. Cho,[53] S.-J. Cho,[134] S.-K. Choi,[22] S. Choudhury,[30] D. Cinabro,[131] L. Corona,[100,43] L. M. Cremaldi,[120] D. Cuesta,[107] S. Cunliffe,[12] T. Czank,[128] N. Dash,[31] F. Dattola,[12] E. De La Cruz-Burelo,[6] G. De Nardo,[97,40] M. De Nuccio,[12] G. De Pietro,[45] R. de Sangro,[39] B. Deschamps,[109] M. Destefanis,[103,46] S. Dey,[91] A. De Yta-Hernandez,[6] A. Di Canto,[3] F. Di Capua,[97,40] S. Di Carlo,[106] J. Dingfelder,[109] Z. Doležal,[7] I. Domínguez Jiménez,[96] T. V. Dong,[18] K. Dort,[50] D. Dossett,[119] S. Dubey,[113] S. Duell,[109] G. Dujany,[107] S. Eidelman,[4,57,74] M. Eliachevitch,[109] D. Epifanov,[4,74] J. E. Fast,[78] T. Ferber,[12] D. Ferlewicz,[119] G. Finocchiaro,[39] S. Fiore,[44] P. Fischer,[114] A. Fodor,[64] F. Forti,[100,43] A. Frey,[19] M. Friedl,[34] B. G. Fulsom,[78] M. Gabriel,[62] N. Gabyshev,[4,74] E. Ganiev,[104,47] M. Garcia-Hernandez,[6] R. Garg,[79] A. Garmash,[4,74] V. Gaur,[130] A. Gaz,[66,67] U. Gebauer,[19] M. Gelb,[51] A. Gellrich,[12] J. Gemmler,[51] T. Geßler,[50] D. Getzkow,[50] R. Giordano,[97,40] A. Giri,[30] A. Glazov,[12] B. Gobbo,[47] R. Godang,[124] P. Goldenzweig,[51] B. Golob,[115,87] P. Gomis,[38] P. Grace,[108] W. Gradl,[49] E. Graziani,[45] D. Greenwald,[90] Y. Guan,[111] C. Hadjivasiliou,[78] S. Halder,[89] K. Hara,[24,21] T. Hara,[24,21] O. Hartbrich,[113] T. Hauth,[51] K. Hayasaka,[73] H. Hayashii,[69] C. Hearty,[110,36] M. Heck,[51]

M. T. Hedges,[113] I. Heredia de la Cruz,[6,11] M. Hernández Villanueva,[120] A. Hershenhorn,[110] T. Higuchi,[128] E. C. Hill,[110] H. Hirata,[66] M. Hoek,[49] M. Hohmann,[119] S. Hollitt,[108] T. Hotta,[77] C.-L. Hsu,[126] Y. Hu,[35] K. Huang,[70] T. Iijima,[66,67] K. Inami,[66] G. Inguglia,[34] J. Irakkathil Jabbar,[51] A. Ishikawa,[24,21] R. Itoh,[24,21] M. Iwasaki,[76] Y. Iwasaki,[24] S. Iwata,[95] P. Jackson,[108] W. W. Jacobs,[32] I. Jaegle,[112] D. E. Jaffe,[3] E.-J. Jang,[22] M. Jeandron,[120] H. B. Jeon,[56] S. Jia,[18] Y. Jin,[47] C. Joo,[128] K. K. Joo,[10] I. Kadenko,[88] J. Kahn,[51] H. Kakuno,[95] A. B. Kaliyar,[89] J. Kandra,[7] K. H. Kang,[56] P. Kapusta,[72] R. Karl,[12] G. Karyan,[133] Y. Kato,[66,67] H. Kawai,[9] T. Kawasaki,[52] T. Keck,[51] C. Ketter,[113] H. Kichimi,[24] C. Kiesling,[62] B. H. Kim,[83] C.-H. Kim,[23] D. Y. Kim,[86] H. J. Kim,[56] J. B. Kim,[54] K.-H. Kim,[134] K. Kim,[54] S.-H. Kim,[83] Y.-K. Kim,[134] Y. Kim,[54] T. D. Kimmel,[130] H. Kindo,[24,21] K. Kinoshita,[111] B. Kirby,[3] C. Kleinwort,[12] B. Knysh,[106] P. Kodyš,[7] T. Koga,[24] S. Kohani,[113] I. Komarov,[12] T. Konno,[52] S. Korpar,[118,87] N. Kovalchuk,[12] T. M. G. Kraetzschmar,[62] P. Križan,[115,87] R. Kroeger,[120] J. F. Krohn,[119] P. Krokovny,[4,74] H. Krüger,[109] W. Kuehn,[50] T. Kuhr,[59] J. Kumar,[5] M. Kumar,[61] R. Kumar,[81] K. Kumara,[131] T. Kumita,[95] T. Kunigo,[24] M. Künzel,[12,59] S. Kurz,[12] A. Kuzmin,[4,74] P. Kvasnička,[7] Y.-J. Kwon,[134] S. Lacaprara,[41] Y.-T. Lai,[128] C. La Licata,[128] K. Lalwani,[61] L. Lanceri,[47] J. S. Lange,[50] K. Lautenbach,[50] P. J. Laycock,[3] F. R. Le Diberder,[106] I.-S. Lee,[23] S. C. Lee,[56] P. Leitl,[62] D. Levit,[90] P. M. Lewis,[109] C. Li,[58] L. K. Li,[111] S. X. Li,[2] Y. M. Li,[35] Y. B. Li,[80] J. Libby,[31] K. Lieret,[59] L. Li Gioi,[62] J. Lin,[70] Z. Liptak,[113] Q. Y. Liu,[12] Z. A. Liu,[35] D. Liventsev,[131,24] S. Longo,[12] A. Loos,[125] P. Lu,[70] M. Lubej,[87] T. Lueck,[59] F. Luetticke,[109] T. Luo,[18] C. MacQueen,[119] Y. Maeda,[66,67] M. Maggiora,[103,46] S. Maity,[28] R. Manfredi,[104,47] E. Manoni,[42] S. Marcello,[103,46] C. Marinas,[38] A. Martini,[102,45] M. Masuda,[15,77] T. Matsuda,[121] K. Matsuoka,[66,67] D. Matvienko,[4,57,74] J. McNeil,[112] F. Meggendorfer,[62] J. C. Mei,[18] F. Meier,[13] M. Merola,[97,40] F. Metzner,[51] M. Milesi,[119] C. Miller,[129] K. Miyabayashi,[69] H. Miyake,[24,21] H. Miyata,[73] R. Mizuk,[57,26] K. Azmi,[117] G. B. Mohanty,[89] H. Moon,[54] T. Moon,[83] J. A. Mora Grimaldo,[127] A. Morda,[41] T. Morii,[128] H.-G. Moser,[62] M. Mrvar,[34] F. Mueller,[62] F. J. Müller,[12] Th. Muller,[51] G. Muroyama,[66] C. Murphy,[128] R. Mussa,[46] K. Nakagiri,[24] I. Nakamura,[24,21] K. R. Nakamura,[24,21] E. Nakano,[76] M. Nakao,[24,21] H. Nakayama,[24,21] H. Nakazawa,[70] T. Nanut,[87] Z. Natkaniec,[72] A. Natochii,[113] M. Nayak,[91] G. Nazaryan,[133] D. Neverov,[66] C. Niebuhr,[12] M. Niiyama,[55] J. Ninkovic,[63] N. K. Nisar,[3] S. Nishida,[24,21] K. Nishimura,[113] M. Nishimura,[24] M. H. A. Nouxman,[117] B. Oberhof,[39] K. Ogawa,[73] S. Ogawa,[92] S. L. Olsen,[22] Y. Onishchuk,[88] H. Ono,[73] Y. Onuki,[127] P. Oskin,[57] E. R. Oxford,[5] H. Ozaki,[24,21] P. Pakhlov,[57,65] G. Pakhlova,[26,57] A. Paladino,[100,43] T. Pang,[122] A. Panta,[120] E. Paoloni,[100,43] S. Pardi,[40] C. Park,[134] H. Park,[56] S.-H. Park,[134] B. Paschen,[109] A. Passeri,[45] A. Pathak,[116] S. Patra,[27] S. Paul,[90] T. K. Pedlar,[60] I. Peruzzi,[39] R. Peschke,[113] R. Pestotnik,[87] M. Piccolo,[39] L. E. Piilonen,[130] P. L. M. Podesta-Lerma,[96] G. Polat,[1] V. Popov,[26] C. Praz,[12] E. Prencipe,[16] M. T. Prim,[109] M. V. Purohit,[75] N. Rad,[12] P. Rados,[12] R. Rasheed,[107] M. Reif,[62] S. Reiter,[50] M. Remnev,[4,74] P. K. Resmi,[31] I. Ripp-Baudot,[107] M. Ritter,[59] M. Ritzert,[114] G. Rizzo,[100,43] L. B. Rizzuto,[87] S. H. Robertson,[64,36] D. Rodríguez Pérez,[96] J. M. Roney,[129,36] C. Rosenfeld,[125] A. Rostomyan,[12] N. Rout,[31] M. Rozanska,[72] G. Russo,[97,40] D. Sahoo,[89] Y. Sakai,[24,21] D. A. Sanders,[120] S. Sandilya,[111] A. Sangal,[111] L. Santelj,[115,87] P. Sartori,[98,41] J. Sasaki,[127] Y. Sato,[93] V. Savinov,[122] B. Scavino,[49]

M. Schram,[78] H. Schreeck,[19] J. Schueler,[113] C. Schwanda,[34] A. J. Schwartz,[111] B. Schwenker,[19] R. M. Seddon,[64] Y. Seino,[73] A. Selce,[101,44] K. Senyo,[132] I. S. Seong,[113] J. Serrano,[1] M. E. Sevior,[119] C. Sfienti,[49] V. Shebalin,[113] C. P. Shen,[2] H. Shibuya,[92] J.-G. Shiu,[70] B. Shwartz,[4,74] A. Sibidanov,[129] F. Simon,[62] J. B. Singh,[79] S. Skambraks,[62] K. Smith,[119] R. J. Sobie,[129,36] A. Soffer,[91] A. Sokolov,[33] Y. Soloviev,[12] E. Solovieva,[57] S. Spataro,[103,46] B. Spruck,[49] M. Starič,[87] S. Stefkova,[12] Z. S. Stottler,[130] R. Stroili,[98,41] J. Strube,[78] J. Stypula,[72] M. Sumihama,[20,77] K. Sumisawa,[24,21] T. Sumiyoshi,[95] D. J. Summers,[120] W. Sutcliffe,[109] K. Suzuki,[66] S. Y. Suzuki,[24,21] H. Svidras,[12] M. Tabata,[9] M. Takahashi,[12] M. Takizawa,[82,25,84] U. Tamponi,[46] S. Tanaka,[24,21] K. Tanida,[48] H. Tanigawa,[127] N. Taniguchi,[24] Y. Tao,[112] P. Taras,[105] F. Tenchini,[12] D. Tonelli,[47] E. Torassa,[41] K. Trabelsi,[106] T. Tsuboyama,[24,21] N. Tsuzuki,[66] M. Uchida,[94] I. Ueda,[24,21] S. Uehara,[24,21] T. Ueno,[93] T. Uglov,[57,26] K. Unger,[51] Y. Unno,[23] S. Uno,[24,21] P. Urquijo,[119] Y. Ushiroda,[24,21,127] Y. Usov,[4,74] S. E. Vahsen,[113] R. van Tonder,[109] G. S. Varner,[113] K. E. Varvell,[126] A. Vinokurova,[4,74] L. Vitale,[104,47] V. Vorobyev,[4,57,74] A. Vossen,[13] E. Waheed,[24] H. M. Wakeling,[64] K. Wan,[127] W. Wan Abdullah,[117] B. Wang,[62] C. H. Wang,[71] M.-Z. Wang,[70] X. L. Wang,[18] A. Warburton,[64] M. Watanabe,[73] S. Watanuki,[106] I. Watson,[127] J. Webb,[119] S. Wehle,[12] M. Welsch,[109] C. Wessel,[109] J. Wiechczynski,[43] P. Wieduwilt,[19] H. Windel,[62] E. Won,[54] L. J. Wu,[35] X. P. Xu,[85] B. Yabsley,[126] S. Yamada,[24] W. Yan,[123] S. B. Yang,[54] H. Ye,[12] J. Yelton,[112] I. Yeo,[53] J. H. Yin,[54] M. Yonenaga,[95] Y. M. Yook,[35] T. Yoshinobu,[73] C. Z. Yuan,[35] G. Yuan,[123] W. Yuan,[41] Y. Yusa,[73] L. Zani,[1] J. Z. Zhang,[35] Y. Zhang,[123] Z. Zhang,[123] V. Zhilich,[4,74] Q. D. Zhou,[66,68] X. Y. Zhou,[2] V. I. Zhukova,[57] V. Zhulanov,[4,74] and A. Zupanc[87]

(Belle II Collaboration)

[1]*Aix Marseille Université, CNRS/IN2P3, CPPM, 13288 Marseille, France*
[2]*Beihang University, Beijing 100191, China*
[3]*Brookhaven National Laboratory, Upton, New York 11973, U.S.A.*
[4]*Budker Institute of Nuclear Physics SB RAS, Novosibirsk 630090, Russian Federation*
[5]*Carnegie Mellon University, Pittsburgh, Pennsylvania 15213, U.S.A.*
[6]*Centro de Investigacion y de Estudios Avanzados del Instituto Politecnico Nacional, Mexico City 07360, Mexico*
[7]*Faculty of Mathematics and Physics, Charles University, 121 16 Prague, Czech Republic*
[8]*Chiang Mai University, Chiang Mai 50202, Thailand*
[9]*Chiba University, Chiba 263-8522, Japan*
[10]*Chonnam National University, Gwangju 61186, South Korea*
[11]*Consejo Nacional de Ciencia y Tecnología, Mexico City 03940, Mexico*
[12]*Deutsches Elektronen–Synchrotron, 22607 Hamburg, Germany*
[13]*Duke University, Durham, North Carolina 27708, U.S.A.*
[14]*Institute of Theoretical and Applied Research (ITAR), Duy Tan University, Hanoi 100000, Vietnam*
[15]*Earthquake Research Institute, University of Tokyo, Tokyo 113-0032, Japan*
[16]*Forschungszentrum Jülich, 52425 Jülich, Germany*
[17]*Department of Physics, Fu Jen Catholic University, Taipei 24205, Taiwan*
[18]*Key Laboratory of Nuclear Physics and Ion-beam Application (MOE) and Institute of Modern Physics, Fudan University, Shanghai 200443, China*

[19]*II. Physikalisches Institut, Georg-August-Universität Göttingen, 37073 Göttingen, Germany*
[20]*Gifu University, Gifu 501-1193, Japan*
[21]*The Graduate University for Advanced Studies (SOKENDAI), Hayama 240-0193, Japan*
[22]*Gyeongsang National University, Jinju 52828, South Korea*
[23]*Department of Physics and Institute of Natural Sciences, Hanyang University, Seoul 04763, South Korea*
[24]*High Energy Accelerator Research Organization (KEK), Tsukuba 305-0801, Japan*
[25]*J-PARC Branch, KEK Theory Center, High Energy Accelerator Research Organization (KEK), Tsukuba 305-0801, Japan*
[26]*Higher School of Economics (HSE), Moscow 101000, Russian Federation*
[27]*Indian Institute of Science Education and Research Mohali, SAS Nagar, 140306, India*
[28]*Indian Institute of Technology Bhubaneswar, Satya Nagar 751007, India*
[29]*Indian Institute of Technology Guwahati, Assam 781039, India*
[30]*Indian Institute of Technology Hyderabad, Telangana 502285, India*
[31]*Indian Institute of Technology Madras, Chennai 600036, India*
[32]*Indiana University, Bloomington, Indiana 47408, U.S.A.*
[33]*Institute for High Energy Physics, Protvino 142281, Russian Federation*
[34]*Institute of High Energy Physics, Vienna 1050, Austria*
[35]*Institute of High Energy Physics, Chinese Academy of Sciences, Beijing 100049, China*
[36]*Institute of Particle Physics (Canada), Victoria, British Columbia V8W 2Y2, Canada*
[37]*Institute of Physics, Vietnam Academy of Science and Technology (VAST), Hanoi, Vietnam*
[38]*Instituto de Fisica Corpuscular, Paterna 46980, Spain*
[39]*INFN Laboratori Nazionali di Frascati, I-00044 Frascati, Italy*
[40]*INFN Sezione di Napoli, I-80126 Napoli, Italy*
[41]*INFN Sezione di Padova, I-35131 Padova, Italy*
[42]*INFN Sezione di Perugia, I-06123 Perugia, Italy*
[43]*INFN Sezione di Pisa, I-56127 Pisa, Italy*
[44]*INFN Sezione di Roma, I-00185 Roma, Italy*
[45]*INFN Sezione di Roma Tre, I-00146 Roma, Italy*
[46]*INFN Sezione di Torino, I-10125 Torino, Italy*
[47]*INFN Sezione di Trieste, I-34127 Trieste, Italy*
[48]*Advanced Science Research Center, Japan Atomic Energy Agency, Naka 319-1195, Japan*
[49]*Johannes Gutenberg-Universität Mainz, Institut für Kernphysik, D-55099 Mainz, Germany*
[50]*Justus-Liebig-Universität Gießen, 35392 Gießen, Germany*
[51]*Institut für Experimentelle Teilchenphysik, Karlsruher Institut für Technologie, 76131 Karlsruhe, Germany*
[52]*Kitasato University, Sagamihara 252-0373, Japan*
[53]*Korea Institute of Science and Technology Information, Daejeon 34141, South Korea*
[54]*Korea University, Seoul 02841, South Korea*
[55]*Kyoto Sangyo University, Kyoto 603-8555, Japan*
[56]*Kyungpook National University, Daegu 41566, South Korea*
[57]*P.N. Lebedev Physical Institute of the Russian Academy of Sciences, Moscow 119991, Russian Federation*
[58]*Liaoning Normal University, Dalian 116029, China*

[59]*Ludwig Maximilians University, 80539 Munich, Germany*
[60]*Luther College, Decorah, Iowa 52101, U.S.A.*
[61]*Malaviya National Institute of Technology Jaipur, Jaipur 302017, India*
[62]*Max-Planck-Institut für Physik, 80805 München, Germany*
[63]*Semiconductor Laboratory of the Max Planck Society, 81739 München, Germany*
[64]*McGill University, Montréal, Québec, H3A 2T8, Canada*
[65]*Moscow Physical Engineering Institute, Moscow 115409, Russian Federation*
[66]*Graduate School of Science, Nagoya University, Nagoya 464-8602, Japan*
[67]*Kobayashi-Maskawa Institute, Nagoya University, Nagoya 464-8602, Japan*
[68]*Institute for Advanced Research, Nagoya University, Nagoya 464-8602, Japan*
[69]*Nara Women's University, Nara 630-8506, Japan*
[70]*Department of Physics, National Taiwan University, Taipei 10617, Taiwan*
[71]*National United University, Miao Li 36003, Taiwan*
[72]*H. Niewodniczanski Institute of Nuclear Physics, Krakow 31-342, Poland*
[73]*Niigata University, Niigata 950-2181, Japan*
[74]*Novosibirsk State University, Novosibirsk 630090, Russian Federation*
[75]*Okinawa Institute of Science and Technology, Okinawa 904-0495, Japan*
[76]*Osaka City University, Osaka 558-8585, Japan*
[77]*Research Center for Nuclear Physics, Osaka University, Osaka 567-0047, Japan*
[78]*Pacific Northwest National Laboratory, Richland, Washington 99352, U.S.A.*
[79]*Panjab University, Chandigarh 160014, India*
[80]*Peking University, Beijing 100871, China*
[81]*Punjab Agricultural University, Ludhiana 141004, India*
[82]*Meson Science Laboratory, Cluster for Pioneering Research, RIKEN, Saitama 351-0198, Japan*
[83]*Seoul National University, Seoul 08826, South Korea*
[84]*Showa Pharmaceutical University, Tokyo 194-8543, Japan*
[85]*Soochow University, Suzhou 215006, China*
[86]*Soongsil University, Seoul 06978, South Korea*
[87]*J. Stefan Institute, 1000 Ljubljana, Slovenia*
[88]*Taras Shevchenko National Univ. of Kiev, Kiev, Ukraine*
[89]*Tata Institute of Fundamental Research, Mumbai 400005, India*
[90]*Department of Physics, Technische Universität München, 85748 Garching, Germany*
[91]*Tel Aviv University, School of Physics and Astronomy, Tel Aviv, 69978, Israel*
[92]*Toho University, Funabashi 274-8510, Japan*
[93]*Department of Physics, Tohoku University, Sendai 980-8578, Japan*
[94]*Tokyo Institute of Technology, Tokyo 152-8550, Japan*
[95]*Tokyo Metropolitan University, Tokyo 192-0397, Japan*
[96]*Universidad Autonoma de Sinaloa, Sinaloa 80000, Mexico*
[97]*Dipartimento di Scienze Fisiche, Università di Napoli Federico II, I-80126 Napoli, Italy*
[98]*Dipartimento di Fisica e Astronomia, Università di Padova, I-35131 Padova, Italy*
[99]*Dipartimento di Fisica, Università di Perugia, I-06123 Perugia, Italy*
[100]*Dipartimento di Fisica, Università di Pisa, I-56127 Pisa, Italy*
[101]*Università di Roma "La Sapienza," I-00185 Roma, Italy*
[102]*Dipartimento di Matematica e Fisica, Università di Roma Tre, I-00146 Roma, Italy*
[103]*Dipartimento di Fisica, Università di Torino, I-10125 Torino, Italy*
[104]*Dipartimento di Fisica, Università di Trieste, I-34127 Trieste, Italy*

[105] *Université de Montréal, Physique des Particules, Montréal, Québec, H3C 3J7, Canada*
[106] *Université Paris-Saclay, CNRS/IN2P3, IJCLab, 91405 Orsay, France*
[107] *Université de Strasbourg, CNRS, IPHC, UMR 7178, 67037 Strasbourg, France*
[108] *Department of Physics, University of Adelaide, Adelaide, South Australia 5005, Australia*
[109] *University of Bonn, 53115 Bonn, Germany*
[110] *University of British Columbia, Vancouver, British Columbia, V6T 1Z1, Canada*
[111] *University of Cincinnati, Cincinnati, Ohio 45221, U.S.A.*
[112] *University of Florida, Gainesville, Florida 32611, U.S.A.*
[113] *University of Hawaii, Honolulu, Hawaii 96822, U.S.A.*
[114] *University of Heidelberg, 68131 Mannheim, Germany*
[115] *Faculty of Mathematics and Physics, University of Ljubljana, 1000 Ljubljana, Slovenia*
[116] *University of Louisville, Louisville, Kentucky 40292, U.S.A.*
[117] *National Centre for Particle Physics, University Malaya, 50603 Kuala Lumpur, Malaysia*
[118] *University of Maribor, 2000 Maribor, Slovenia*
[119] *School of Physics, University of Melbourne, Victoria 3010, Australia*
[120] *University of Mississippi, University, Mississippi 38677, U.S.A.*
[121] *University of Miyazaki, Miyazaki 889-2192, Japan*
[122] *University of Pittsburgh, Pittsburgh, Pennsylvania 15260, U.S.A.*
[123] *University of Science and Technology of China, Hefei 230026, China*
[124] *University of South Alabama, Mobile, Alabama 36688, U.S.A.*
[125] *University of South Carolina, Columbia, South Carolina 29208, U.S.A.*
[126] *School of Physics, University of Sydney, New South Wales 2006, Australia*
[127] *Department of Physics, University of Tokyo, Tokyo 113-0033, Japan*
[128] *Kavli Institute for the Physics and Mathematics of the Universe (WPI), University of Tokyo, Kashiwa 277-8583, Japan*
[129] *University of Victoria, Victoria, British Columbia, V8W 3P6, Canada*
[130] *Virginia Polytechnic Institute and State University, Blacksburg, Virginia 24061, U.S.A.*
[131] *Wayne State University, Detroit, Michigan 48202, U.S.A.*
[132] *Yamagata University, Yamagata 990-8560, Japan*
[133] *Alikhanyan National Science Laboratory, Yerevan 0036, Armenia*
[134] *Yonsei University, Seoul 03722, South Korea*

Abstract

We utilize a sample of $34.6\,\mathrm{fb}^{-1}$, collected by the Belle II experiment at the SuperKEKB asymmetric energy e^+e^- collider, to search for the $B^+ \to \phi K^+$, $B^+ \to \phi K^{*+}$, $B^0 \to \phi K^0_S$, and $B^0 \to \phi K^{*0}$ decays. Charmless hadronic B decays represent an important part of the Belle II physics program, and are an ideal benchmark to test the detector capabilities in terms of tracking efficiency, charged particle identification, vertexing, and advanced analysis techniques. Each channel is observed with a significance that exceeds 5 standard deviations, and we obtain measurements of their branching ratios that are in good agreement with the world averages. For the $B \to \phi K^*$ modes, we also perform a measurement of the longitudinal polarization fraction f_L.

I. INTRODUCTION

The $B^0 \to \phi K^0$ channel is one of the most interesting among the charmless hadronic B decays, as it proceeds dominantly through penguin amplitudes, and is theoretically well understood [1]. The time dependent CP violation analysis of this mode may reveal effects of physics beyond the standard model, in case some significant deviation (from the tree dominated $B^0 \to J/\psi K^0$) is observed.

The size of the dataset collected so far by the Belle II experiment does not yet allow for such an analysis, so as a preparatory work we focus on the rediscovery of this and of the isospin related $B^+ \to \phi K^+$ mode. The relevance of this work consists in the fact that these decays have branching fractions below 10^{-5} and suffer from relatively high combinatorial backgrounds, mostly arising from random combination of particles in *continuum* $e^+e^- \to q\overline{q}$ ($q = u, d, s, c$) events. The rediscovery of these modes thus constitutes an important benchmark for assessing the performance of the detector in terms of tracking efficiency, charged particle identification, vertexing, reconstruction of intermediate resonances, and advanced analysis techniques. The suppression of the continuum background relies on multivariate binary discriminators and the extraction of the signal yield is performed through a multidimensional extended maximum likelihood fit.

The inclusion of the vector-vector $B \to \phi K^*$ channels, which have similar branching fractions, extends the scope of the analysis and allows for a significant measurement of the longitudinal polarization fraction f_L. In the early 2000's, this quantity attracted significant interest (the so-called *polarization puzzle*) as many B decays to pairs of vector mesons that proceed predominantly through penguin amplitudes have been observed to have sizable transverse polarization, contrary to naïve predictions based on helicity arguments, which predict $f_L \sim 1$ (see e.g. the section *Polarization in B decays* in [2]). The general consensus nowadays is that the polarization puzzle can be explained satisfactorily without invoking effects of physics beyond the standard model (for example by postulating large contributions from penguin annihilation [3] or electroweak penguin [4] diagrams). Still, the measurement of the polarization is very interesting for us as it is very sensitive to effects produced by the non-uniform detector acceptance; demonstrating the capability of producing an accurate measurement is another important milestone for the experiment.

II. THE BELLE II DETECTOR AND DATASET

The Belle II detector is described in detail in Ref. [5]. The innermost sub-detector is the vertex detector (VXD), devoted to tracking and vertexing, which is comprised of two layers of silicon pixel sensors surrounded by four layers of silicon strips. The main tracking device is a small-cell, helium ethane based, central drift chamber (CDC), which precisely measures the momenta of charged particles and their specific energy loss due to ionization (dE/dx). Additional particle identification (PID) is provided by two Cherenkov detectors: the Time Of Propagation (TOP) counter in the barrel region, and the Aerogel Ring Imaging CHerenkov (ARICH), which covers the forward endcap region. Photon detection and electron identification are provided by a CsI(Tl) electromagnetic calorimeter (ECL). All these subdetectors operate in a 1.5T magnetic field generated by a superconducting solenoid. The axis of the solenoid defines the z axis of the laboratory reference frame, and its positive direction coincides approximately with the momentum of the electron beam. The iron return yoke, instrumented with scintillator strips and resistive-plate chambers, constitutes the

KLM, the sub-detector devoted to the identification of muons and K_L mesons.

Operations with the complete Belle II detector at the SuperKEKB asymmetric energy e^+e^- collider [6] began in March 2019. We utilize the data collected until the first half of May 2020 at the center-of-mass (CM) energy corresponding to the mass of the $\Upsilon(4S)$ resonance. The sample has an integrated luminosity of $34.6\,\text{fb}^{-1}$, which corresponds to 19.7 million B^+B^- and 18.7 million $B^0\overline{B}^0$ pairs. We derived the above numbers by taking the $e^+e^- \to \Upsilon(4S)$ cross-section (1.110 ± 0.008) nb [7], assuming that the $\Upsilon(4S)$ decays exclusively to $B\overline{B}$ pairs, and $f_{00} = 0.487 \pm 0.010 \pm 0.08$ [8], where f_{00} is the branching fraction of $\Upsilon(4S) \to B^0\overline{B}^0$.

III. EVENT SELECTION AND ANALYSIS VARIABLES

We search for the final states $B^+ \to \phi K^+$, $B^+ \to \phi K^{*+}$, $B^0 \to \phi K^0_S$, and $B^0 \to \phi K^{*0}$, with $\phi \to K^+K^-$, $K^{*0} \to K^+\pi^-$, $K^{*+} \to K^0_S\pi^+$, and $K^0_S \to \pi^+\pi^-$. Unless otherwise stated, charge conjugation is always implied.

Signal candidates are selected by applying the following criteria. Charged tracks expected to originate from the interaction point (thus excluding the daughters of K^0_S candidates) are required to have their point of closest approach within 2 cm (0.5 cm) of the measured e^+e^- interaction point along the z axis (in the transverse plane). Charged kaon candidates are selected by applying a cut on a likelihood based binary $K - \pi$ discriminator, which combines PID information from all the subdetectors that can provide useful information. For the bachelor kaon in $B^+ \to \phi K^+$ and for the kaon from the $K^{*0} \to K^+\pi^-$, we apply a loose requirement (whose typical efficiency is $> 90\%$ in the relevant momentum and polar angle ranges), whereas for the ϕ candidate reconstruction, we require that at least one of the daughter kaons satisfies a tighter (efficiency $> 80\%$) selection.

The invariant masses of the intermediate resonances must satisfy: $1.00 < m(\phi) < 1.05$ GeV/c^2, $0.485 < m(K^0_S) < 0.510$ GeV/c^2, and $0.74 < m(K\pi) < 0.94$ GeV/c^2 (the latter requirement being valid for both K^{*+} and K^{*0} candidates).

To greatly enhance the purity of the K^0_S sample, we compute the *significance of distance* of each candidate, by taking the ratio between the length of the segment that connects the interaction point with the reconstructed K^0_S decay vertex and the uncertainty in the determination of the decay vertex. We retain candidates in which the significance of distance is greater than 50 (this requirement having an efficiency $> 80\%$). Figure 1 shows the distributions of the invariant mass of the K^0_S candidates, and that of the significance of distance, separately for genuine K^0_S candidates and random pion pair combinations.

To reduce the dominant backgrounds arising from random combinations of particles in continuum events, we consider the ratio of the second to zeroth Fox-Wolfram moments (R_2) [9] and the cosine of the angle between the thrust axis of the signal B candidate and that of the rest of the event (cosTBTO). We require $R_2 < 0.5$ and cosTBTO < 0.95. These cuts are quite loose, to keep the signal reconstruction efficiency as high as reasonably possible. We then combine 30 variables sensitive to the event shape and train a multivariate BDT discriminator to distinguish between signal events (which are typically *spherical*) and continuum events (more *jet-like*). The discriminator is optimized for each individual final state, and it is utilized as one of the input variables in the final maximum likelihood fit.

As in most analyses in which the signal B candidate is fully reconstructed, we use the standard beam-constrained mass M_{bc} and the difference between the reconstructed and

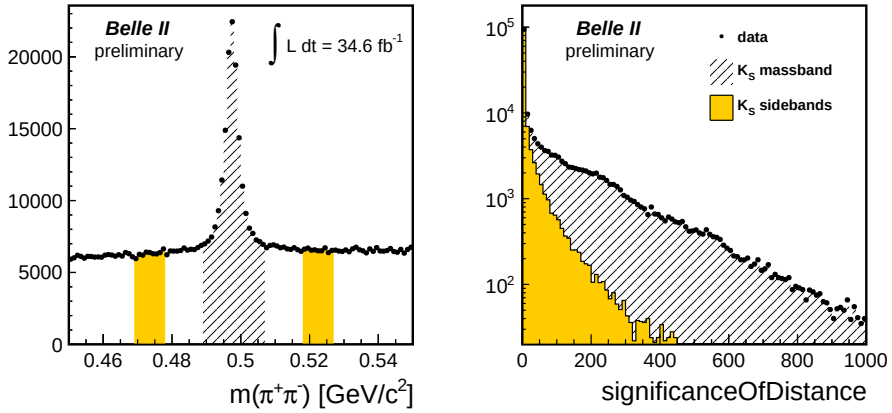

FIG. 1. Left figure: invariant mass of the K_S^0 candidates, and definition of the massband (hatched region) and sidebands (colored region). Right: distribution of the significance of distance for the K_S^0 massband (data points and hatched histogram) overlaid with the distribution taken from the sidebands (colored histogram).

expected B candidate energies ΔE:

$$M_{\rm bc} = \sqrt{E^{*2}_{\rm beam}c^4 - p^{*2}_B c^2}\ , \tag{1}$$

$$\Delta E = E^*_B - E^*_{\rm beam}\ , \tag{2}$$

where (E^*_B, p^*_B) are the measured energy and momentum of the candidate B, and $E^*_{\rm beam} = \sqrt{s}/2$. All quantities are calculated in the CM system. For the final fit, we require that candidates satisfy $M_{\rm bc} > 5.25$ GeV/c^2 and $|\Delta E| < 0.2$ GeV.

For $B \to V_1 V_2$ decays, where V_i is a vector meson decaying to two pseudoscalar mesons, the angular distribution, after integrating over the angle between the decay planes of V_1 and V_2, is described by:

$$\frac{1}{\Gamma}\frac{d^2\Gamma}{d\cos\theta_1 d\cos\theta_2} = \frac{9}{4}\left[\frac{1}{4}(1-f_L)\sin^2\theta_1\sin^2\theta_2 + f_L\cos^2\theta_1\cos^2\theta_2\right]\ , \tag{3}$$

where the subscript L refers to the longitudinally polarized component, and f_L is the fraction of the longitudinally polarized component.

For the ϕ and K^* resonances, the helicity angles $\theta_{H,\phi}$ and θ_{H,K^*} are defined as the angle between the momentum of the daughter kaon (the negatively charged in the case of the ϕ, the only kaon in the case of the K^*) and the flight direction of the ϕ/K^*, as measured in the ϕ/K^* rest frame.

The helicity angles $\theta_{H,\phi}$ and θ_{H,K^*} are the key variables for the measurement of the longitudinal polarization fraction f_L. In the case of $B \to \phi K$, where the spin of the ϕ is forced by angular momentum conservation to be perpendicular to the ϕ momentum, the variable $\theta_{H,\phi}$ provides additional discrimination against the continuum background and the nonresonant $B \to K^+K^-K$ component; for both backgrounds, the $\cos\theta_{H,\phi}$ distribution is expected to be roughly flat.

The distributions of $\cos\theta_{H,\phi}$ and (in a higher measure) $\cos\theta_{H,K^*}$ are distorted from the ideal theoretical probability density functions (pdf's) by effects related to the non-uniform

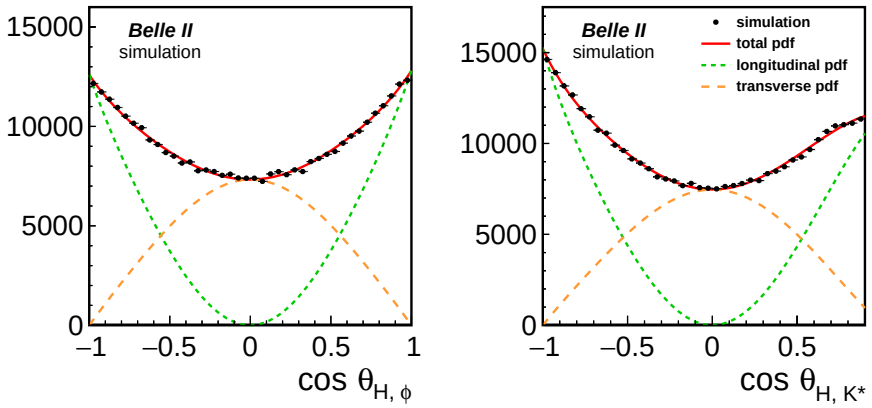

FIG. 2. Distributions of $\cos\theta_{H,\phi}$ (left) and $\cos\theta_{H,K^*}$ (right) taken from the simulation, generated with the $f_L = 0.5$ hypothesis and no background. The green dashed (orange long dashed) lines show the pdf's of the longitudinal (transverse) components, while the red solid lines is the sum of the two. The distortion due to acceptance effects on the right side of the $\cos\theta_{H,K^*}$ distribution is clearly visible.

acceptance of the detector and other selection criteria. The events with $\cos\theta_{H,K^*} > 0.9$ are particularly affected by these kinds of effects and are therefore discarded for the final fit. Figure 2 shows the expected distributions for these variables, for correctly reconstructed signal events for the hypothesis $f_L = 0.5$.

For each decay mode, we accept at most one signal candidate per event. If an event contains more than one candidate (which happens very rarely for $B \to \phi K$ and $\sim 10\%$ of the times for $B \to \phi K^*$), we retain the candidate with highest vertex probability for the signal B candidate. We verify in the simulation that this choice significantly improves the purity of the sample.

IV. MAXIMUM LIKELIHOOD FIT

The extraction of the quantities of interest is performed using an unbinned multivariate maximum likelihood (ML) fit. For the i^{th} input event, the likelihood $\mathcal{L}_i$ is defined as:

$$\mathcal{L}_i = \sum_{j=1}^{m} n_j \mathcal{P}_j(\mathbf{x}_i) \ , \tag{4}$$

where $\mathcal{P}_j$ is the probability for the hypothesis (component) j evaluated for the input variables $\mathbf{x}_i$, and n_j is the number of events in the whole sample for the component j (m being the total number of components considered in the fit). The probability $\mathcal{P}_j$ is the product of the one-dimensional probability density functions for each of the observables (input variables). One of the main assumptions of the analysis is that the correlations among these variables are negligible.

For N input events, the overall likelihood $\mathcal{L}$ is:

$$\mathcal{L} = \frac{e^{-(\sum n_j)}}{N!} \prod_{i=1}^{N} \mathcal{L}_i \ , \tag{5}$$

where the first term takes into account the Poisson fluctuations in the total number of events.

The input variables entering the ML fit are:

1. $M_{\rm bc}$;
2. ΔE;
3. $C'_{\rm out}$ (the transformed output of the continuum suppression multivariate discriminator $C_{\rm out}$);
4. $m(K^+K^-)$ (invariant mass of the ϕ candidate);
5. $\cos\theta_{H,\phi}$ (cosine of the helicity angle of the ϕ candidate);
6. $m(K^+\pi)$ (invariant mass of the K^* candidate);
7. $\cos\theta_{H,K^*}$ (cosine of the helicity angle of the K^* candidate).

The last two variables are relevant only for the $B \to \phi K^*$ modes.

The components considered in the fit are:

- **correctly reconstructed signal events**. For the $B \to \phi K^*$ analysis, we float separately the yields of the longitudinal (N_L) and transverse (N_T) components, and compute f_L taking into account the different reconstruction efficiencies ε_L and ε_T for the longitudinally and transversely polarized events, respectively:

$$f_L = \frac{N_L/\varepsilon_L}{N_L/\varepsilon_L + N_T/\varepsilon_T} \, . \tag{6}$$

  The yield parameters are allowed to take negative values (thus the result on f_L may be outside the physical $[0,1]$ range);

- **self-crossfeed (SXF)**. This component is constituted of signal events in which one or more candidate particles originate from the unreconstructed B. For the $B \to \phi K$ analyses, the fraction of self-crossfeed events is negligible, so this component is not considered;

- **nonresonant**, given by $B \to K^+K^-K^{(*)}$ events. Early BaBar [10] and Belle [11] analyses have shown that this component accounts for (10%) of the events observed in the ϕ mass region; this justifies a separate treatment for this category of events;

- **other $B\overline{B}$ backgrounds**;

- **continuum background**, by far the dominant source of background for this analysis.

The continuum background is modeled from the data, excluding the *signal box* defined by the requirements $M_{\rm bc} > 5.27$ GeV/c^2 and $|\Delta E| < 0.1$ GeV. The pdf's of all the other components are determined from the simulation ([12], [13]).

In the nominal fit, we allow the yields of the signal component(s) and of the continuum background, to vary, along with the following parameters describing the shape of the continuum background: the slope of the Argus function [14] that is used to fit the $M_{\rm bc}$ distribution; the slopes of the (non peaking) ΔE, $m(K^+K^-)$, and $m(K^+\pi)$ components; the fractions of the peaking components in the $m(K^+K^-)$ and $m(K^+\pi)$ distributions; and the mean of the core Gaussian component of the $C'_{\rm out}$ variable.

The shapes and normalization of the SXF, nonresonant, and other $B\overline{B}$ background components are fixed to the expectations from the simulation. The yield of the nonresonant component is fixed to 10% of the (total) signal yield; the fraction of the SXF component relative to the correctly reconstructed signal is kept constant to the predictions of the simulation; and the yield of the other $B\overline{B}$ backgrounds is set to the value predicted by the generic Monte Carlo. All these quantities are varied separately by $\pm 50\%$ for the determination of the systematic uncertainties.

The fitting procedure has been tested extensively using toy Monte Carlo experiments that preserve the correlations (if any) among the input variables and thus test the main assumption of the fit model, which assumes all correlations to be negligible. No significant bias has been detected.

The events in the *signal box* have not been analyzed until the fit procedure was clearly defined, and full confidence was reached from studies on the simulation and data sidebands.

V. RESULTS

Tables I and II summarize the results of the ML fit applied to the Summer 2020 Belle II dataset. In all cases, we see a significant signal, whose significance (taking only into account the statistical uncertainties) ranges from 6.4 to 11.5 standard deviations. The longitudinal polarization fraction in the $B \to \phi K^*$ modes f_L is very consistent with the expectations. The branching ratios have been computed using the formula:

$$\mathcal{B}(B \to X) = \frac{N_{sig}}{N(B\overline{B}) \times 2 \times \varepsilon \times \text{ProdBF}}\,, \tag{7}$$

where N_{sig} is the number of fitted signal events, $N(B\overline{B})$ is the number of (charged or neutral) $B\overline{B}$ pairs, ε is the signal reconstruction efficiency, and ProdBF is the product of the branching fractions of all the intermediate resonances involved. For the $B \to \phi K^*$ modes, the branching ratio is the sum of the partial branching ratios for the longitudinal and transverse components, which have different reconstruction efficiencies.

In general, the results are in good agreement with the world averages [2]. The observed branching fraction of $B \to \phi K^*$ is approximately two standard deviations higher than the average of the previous results. We checked the stability of the fit by discarding in turn one of the input variables: in all cases the variations of the signal yield are less than two events, much smaller than the statistical uncertainty. We also perform a test in which we remove both helicity angles (so that we lose sensitivity to the polarization), and again the fitted yield is quite compatible with the nominal fit. We conclude that the fit is stable, and the higher than expected branching ratio is probably due to a statistical fluctuation.

TABLE I. Summary of the fit results of the $B \to \phi K$ modes. The upper part shows the information about the yields (with statistical uncertainty only) of the signal (`nSig`), SXF (`nSXF`), nonresonant (`nNR`), and other $B\overline{B}$ backgrounds (`nBBbar`) components. The bottom part displays the reconstruction efficiencies and the measured branching fractions.

	$B^+ \to \phi K^+$	$B^0 \to \phi K^0_S$
Events in fit	1576	695
`nSig`	55.0 ± 8.9	15.7 ± 4.9
`nSXF`	0.0 (fixed)	0.0 (fixed)
`nNR`	5.4 (fixed)	1.6 (fixed)
`nBBbar`	13.0 (fixed)	3.4 (fixed)
Significance (stat. only)	11.5σ	6.4σ
ε (%)	42.5 ± 3.0	41.9 ± 4.8
$\mathcal{B}(\times 10^{-6})$	$6.7 \pm 1.1 \pm 0.5$	$3.0 \pm 0.9 \pm 0.4$

TABLE II. Summary of the fit results of the $B \to \phi K^*$ modes. The upper part shows the information about the yields (with statistical uncertainty only) of the longitudinally polarized signal (`nSigL`), transversely polarized signal (`nSigT`), SXF (`nSXF`), nonresonant (`nNR`), and other $B\overline{B}$ backgrounds (`nBBbar`) components. The bottom part displays the reconstruction efficiencies, the measured branching fractions, and longitudinal polarization fractions f_L.

	$B^+ \to \phi K^{*+}$	$B^0 \to \phi K^{*0}$
Events in fit	2133	3055
`nSigL`	17.6 ± 5.7	25.0 ± 7.0
`nSigT`	15.2 ± 5.5	22.7 ± 7.1
`nSXF`	3.7 (fixed)	4.8 (fixed)
`nNR`	3.3 (fixed)	4.7 (fixed)
`nBBbar`	22.6 (fixed)	38.2 (fixed)
Significance (stat. only)	6.4σ	9.8σ
ε_L (%)	31.4 ± 2.5	32.7 ± 1.9
ε_T (%)	36.8 ± 2.9	38.6 ± 2.3
$\mathcal{B}(\times 10^{-6})$	$21.7 \pm 4.6 \pm 1.9$	$11.0 \pm 2.1 \pm 1.1$
f_L	$0.58 \pm 0.23 \pm 0.02$	$0.57 \pm 0.20 \pm 0.04$

Figures 3–6 show the projection plots of the fit variables utilized for each channel. In order to enhance the signal component, a cut on the likelihood ratio (for signal over all the hypotheses, with the likelihood being computed using all the variables with the exception of the one plotted) at 0.5 has been applied.

Finally, we evaluate the compatibility of our results for f_L with the extreme hypotheses $f_L = 0$ and $f_L = 1$. To do this, we respectively fix to 0 the yield of the longitudinal and transverse component, and compute $\sqrt{-2(\log \mathcal{L} - \log \mathcal{L}_0)}$, where $\mathcal{L}$ is the value of the likelihood computed for the tested hypothesis, and $\mathcal{L}_0$ is the likelihood of the nominal fit. The lowest significance ($\sim 4.6\sigma$) is observed for $f_L = 1$ in the $B^+ \to \phi K^{*+}$ channel; in all other cases, the significance exceeds 5σ.

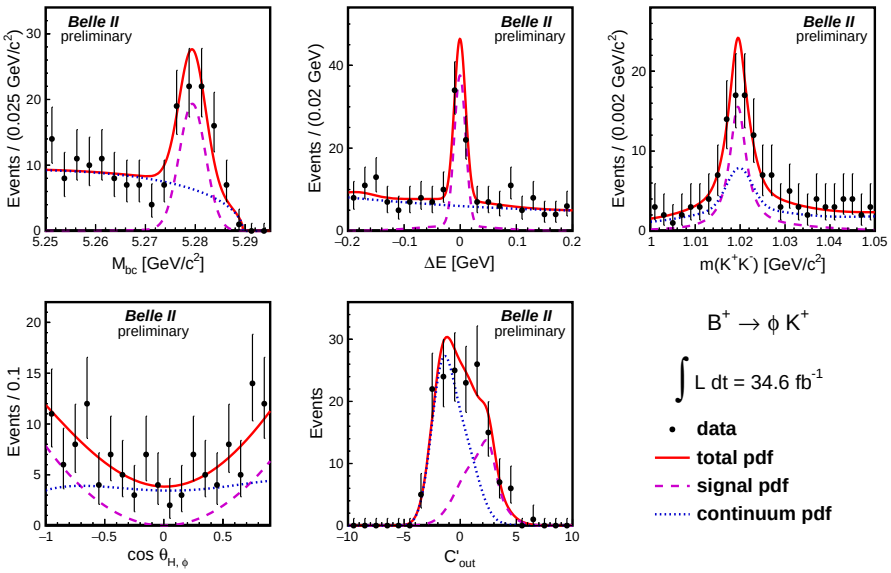

FIG. 3. Signal enhanced projection plots for the fit variables of $B^+ \to \phi K^+$. The solid red curve represents the total fit function, the magenta dashed line shows the signal component, and the blue dotted line corresponds to the continuum background.

VI. SYSTEMATICS

Tables III and IV summarize the systematic uncertainties affecting the measurements of the branching ratios and of f_L, respectively.

TABLE III. Summary of the systematic uncertainties, in per cent, affecting the signal yields. The uncertainties are categorized as multiplicative (M) or additive (A).

Source	$B^+ \to \phi K^+$	$B^+ \to \phi K^{*+}$	$B^0 \to \phi K^0_S$	$B^0 \to \phi K^{*0}$
Tracking efficiency (M)	2.7	4.6	3.6	3.6
K^0_S reconstruction efficiency (M)	–	6.3	10.8	–
Kaon ID efficiency (M)	6.4	1.1	1.0	4.7
Number of $B\overline{B}$ events (M)	2.7	2.7	2.7	2.7
Modeling of $C_{\mathrm{out}'}$ (A)	1.3	1.2	1.0	5.9
$B\overline{B}$ background yield (A)	0.3	1.2	1.4	2.3
Nonresonant yield (A)	3.1	1.8	4.5	3.2
SXF fraction (A)	–	0.6	–	1.0
Total multiplicative	7.5	8.3	11.7	6.5
Total additive	3.4	2.5	4.8	7.1
Total	8.2	8.7	12.7	9.7

We consider the following sources of systematics:

- **tracking efficiency**: we (linearly) add 0.91% for each charged track in the signal final state;

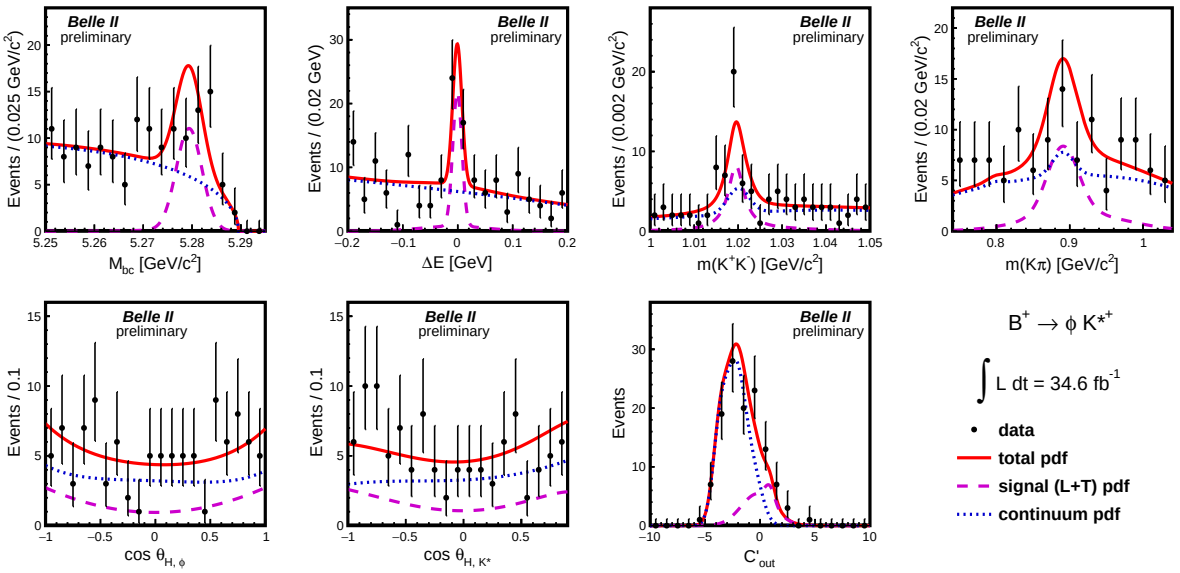

FIG. 4. Signal enhanced projection plots for the fit variables of $B^+ \to \phi K^{*+}$. The solid red curve represents the total fit function, the magenta dashed line shows the signal component, and the blue dotted line corresponds to the continuum background.

TABLE IV. Summary of the systematic uncertainties (expressed in absolute values) affecting the measurement of f_L in the $B \to \phi K^*$ modes.

Source	$B^+ \to \phi K^{*+}$	$B^0 \to \phi K^{*0}$
Acceptance function	0.014	0.007
Modeling of $C_{\text{out}'}$	0.001	0.035
$B\overline{B}$ background yield	0.002	0.009
Nonresonant yield	0.006	0.008
SXF fraction	0.001	0.003
Total	0.015	0.038

- K^0_S **reconstruction efficiency**: we use a data control sample, and we observe that the K^0_S reconstruction efficiency decreases (compared to the simulation) linearly with the flight length. We apply an uncertainty of 1% for each cm of average flight length of the K^0_S candidate;

- **charged kaon identification**: we take the difference between the reconstruction efficiency for signal candidates measured using only Monte Carlo information and the efficiency obtained by shifting the kaon identification efficiency to what is measured on a data sample of $D^{*+} \to \pi^+ D^0 (\to K^-\pi^+)$. This uncertainty is larger for the ϕK^+ and ϕK^{*0} mode, as the charged kaon typically has a much higher momentum than the kaons produced by the ϕ decay, and the agreement between data and simulation is currently much better at lower momenta;

- **number of** $B\overline{B}$ **events**: we assign a 2.7% systematic error, which includes the uncer-

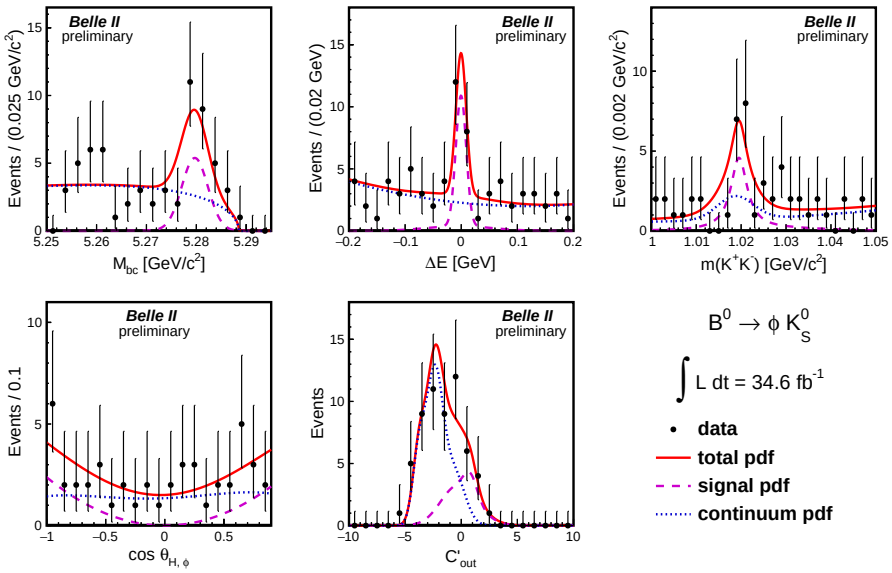

FIG. 5. Signal enhanced projection plots for the fit variables of $B^0 \to \phi K^0_S$. The solid red curve represents the total fit function, the magenta dashed line shows the signal component, and the blue dotted line corresponds to the continuum background.

tainty on cross-section, integrated luminosity, and potential shifts from the peak CM energy during the run periods;

- **modeling of the $C_{\text{out}'}$ variable**: we take the difference in the results obtained when the shape of the $C_{\text{out}'}$ is determined from the data sidebands (nominal fit) and when the shape is modeled from the simulation;

- **yields of SXF, nonresonant, and $B\overline{B}$ background components**: we individually vary by $\pm 50\%$ the yield of each component, and take the difference of the results (with respect to the nominal fit) as systematic uncertainty;

- **acceptance function for the helicity angles** (relevant only for the measurement of f_L). The pdf's of $\cos\theta_{H,\phi}$ and $\cos\theta_{H,K^*}$ are the products of a theoretical pdf's and an acceptance function. We evaluate the systematic uncertainty by taking the difference between the nominal fit results and the cases in which the deviations from unity of the acceptance function are doubled or removed (uniform acceptance).

VII. CONCLUSIONS

In conclusion, we have observed all four $B \to \phi K^{(*)}$ channels in the Summer 2020 Belle II dataset of $34.6\,\text{fb}^{-1}$, with branching ratios that are in good or fair (for the $B^+ \to \phi K^{*+}$ case) agreement with the world averages [2]. The measurement of the longitudinal polarization fraction f_L is in excellent agreement with our expectations.

The results of this analysis are summarized in Table V. We also compute the isospin

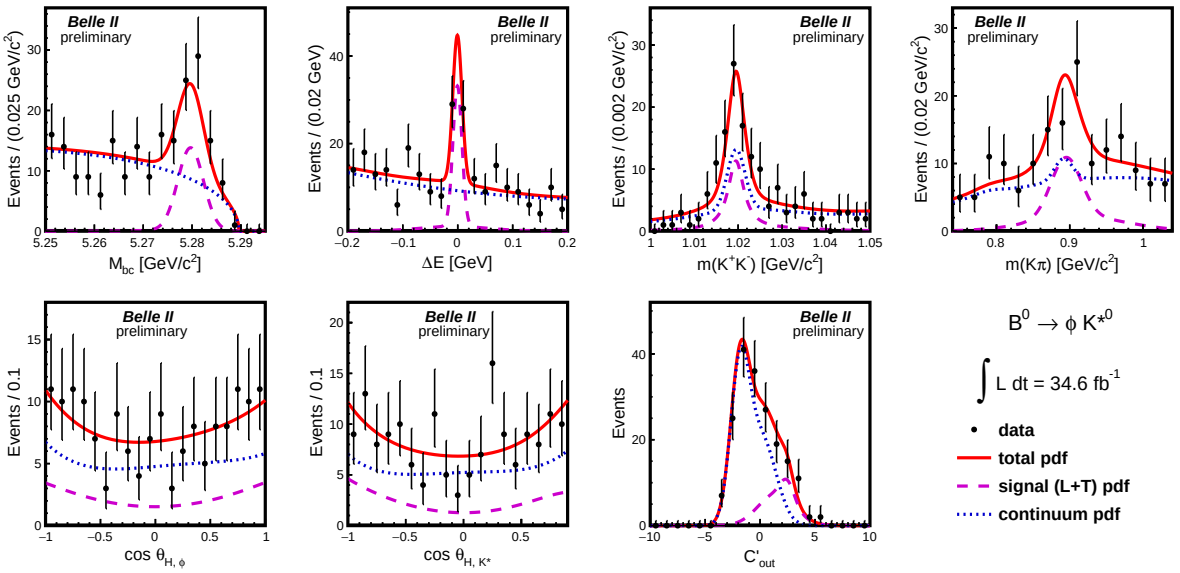

FIG. 6. Signal enhanced projection plots for the fit variables of $B^0 \to \phi K^{*0}$. The solid red curve represents the total fit function, the magenta dashed line shows the signal component, and the blue dotted line corresponds to the continuum background.

ratios

$$I_{\phi K^{(*)}} = \frac{\mathcal{B}(B^+ \to \phi K^{(*)+})}{\mathcal{B}(B^0 \to \phi K^{(*)0})}\,, \tag{8}$$

which are interesting observables for detecting signs of physics beyond the standard model (e.g. in [15]) and that we measure to be in reasonably good agreement with unity.

TABLE V. Summary of the results obtained in this analysis.

	This analysis	World Average [2]
$\mathcal{B}(\times 10^{-6})$		
ϕK^+	$6.7 \pm 1.1 \pm 0.5$	8.8 ± 0.7
ϕK^0	$5.9 \pm 1.8 \pm 0.7$	7.3 ± 0.7
$I_{\phi K}$	$1.1 \pm 0.4 \pm 0.2$	1.21 ± 0.15
ϕK^{*+}	$21.7 \pm 4.6 \pm 1.9$	10.0 ± 2.0
ϕK^{*0}	$11.0 \pm 2.1 \pm 1.1$	10.0 ± 0.5
$I_{\phi K^*}$	$2.0 \pm 0.6 \pm 0.3$	1.00 ± 0.21
f_L		
ϕK^{*+}	$0.58 \pm 0.23 \pm 0.02$	0.50 ± 0.05
ϕK^{*0}	$0.57 \pm 0.20 \pm 0.04$	0.497 ± 0.017

ACKNOWLEDGEMENTS

We thank the SuperKEKB group for the excellent operation of the accelerator; the KEK cryogenics group for the efficient operation of the solenoid; and the KEK computer group for on-site computing support. This work was supported by the following funding sources: Science Committee of the Republic of Armenia Grant No. 18T-1C180; Australian Research Council and research grant Nos. DP180102629, DP170102389, DP170102204, DP150103061, FT130100303, and FT130100018; Austrian Federal Ministry of Education, Science and Research, and Austrian Science Fund No. P 31361-N36; Natural Sciences and Engineering Research Council of Canada, Compute Canada and CANARIE; Chinese Academy of Sciences and research grant No. QYZDJ-SSW-SLH011, National Natural Science Foundation of China and research grant Nos. 11521505, 11575017, 11675166, 11761141009, 11705209, and 11975076, LiaoNing Revitalization Talents Program under contract No. XLYC1807135, Shanghai Municipal Science and Technology Committee under contract No. 19ZR1403000, Shanghai Pujiang Program under Grant No. 18PJ1401000, and the CAS Center for Excellence in Particle Physics (CCEPP); the Ministry of Education, Youth and Sports of the Czech Republic under Contract No. LTT17020 and Charles University grants SVV 260448 and GAUK 404316; European Research Council, 7th Framework PIEF-GA-2013-622527, Horizon 2020 Marie Sklodowska-Curie grant agreement No. 700525 'NIOBE,' and Horizon 2020 Marie Sklodowska-Curie RISE project JENNIFER2 grant agreement No. 822070 (European grants); L'Institut National de Physique Nucléaire et de Physique des Particules (IN2P3) du CNRS (France); BMBF, DFG, HGF, MPG, AvH Foundation, and Deutsche Forschungsgemeinschaft (DFG) under Germany's Excellence Strategy – EXC2121 "Quantum Universe"' – 390833306 (Germany); Department of Atomic Energy and Department of Science and Technology (India); Israel Science Foundation grant No. 2476/17 and United States-Israel Binational Science Foundation grant No. 2016113; Istituto Nazionale di Fisica Nucleare and the research grants BELLE2; Japan Society for the Promotion of Science, Grant-in-Aid for Scientific Research grant Nos. 16H03968, 16H03993, 16H06492, 16K05323, 17H01133, 17H05405, 18K03621, 18H03710, 18H05226, 19H00682, 26220706, and 26400255, the National Institute of Informatics, and Science Information NETwork 5 (SINET5), and the Ministry of Education, Culture, Sports, Science, and Technology (MEXT) of Japan; National Research Foundation (NRF) of Korea Grant Nos. 2016R1D1A1B01010135, 2016R1D1A1B02012900, 2018R1A2B3003643, 2018R1A6A1A06024970, 2018R1D1A1B07047294, 2019K1A3A7A09033840, and 2019R1I1A3A01058933, Radiation Science Research Institute, Foreign Large-size Research Facility Application Supporting project, the Global Science Experimental Data Hub Center of the Korea Institute of Science and Technology Information and KREONET/GLORIAD; Universiti Malaya RU grant, Akademi Sains Malaysia and Ministry of Education Malaysia; Frontiers of Science Program contracts FOINS-296, CB-221329, CB-236394, CB-254409, and CB-180023, and SEP-CINVESTAV research grant 237 (Mexico); the Polish Ministry of Science and Higher Education and the National Science Center; the Ministry of Science and Higher Education of the Russian Federation, Agreement 14.W03.31.0026; University of Tabuk research grants S-1440-0321, S-0256-1438, and S-0280-1439 (Saudi Arabia); Slovenian Research Agency and research grant Nos. J1-9124 and P1-0135; Agencia Estatal de Investigacion, Spain grant Nos. FPA2014-55613-P and FPA2017-84445-P, and CIDEGENT/2018/020 of Generalitat Valenciana; Ministry of Science and Technology and research grant Nos. MOST106-2112-M-002-005-MY3 and MOST107-2119-M-002-035-MY3, and the Ministry of Education (Taiwan); Thailand Cen-

ter of Excellence in Physics; TUBITAK ULAKBIM (Turkey); Ministry of Education and Science of Ukraine; the US National Science Foundation and research grant Nos. PHY-1807007 and PHY-1913789, and the US Department of Energy and research grant Nos. DE-AC06-76RLO1830, DE-SC0007983, DE-SC0009824, DE-SC0009973, DE-SC0010073, DE-SC0010118, DE-SC0010504, DE-SC0011784, DE-SC0012704; and the National Foundation for Science and Technology Development (NAFOSTED) of Vietnam under contract No 103.99-2018.45.

[1] W. Altmannshofer *et al.* (Belle-II), PTEP **2019**, 123C01 (2019), [Erratum: PTEP 2020, 029201 (2020)], arXiv:1808.10567 [hep-ex].
[2] M. Tanabashi *et al.* (Particle Data Group), Phys. Rev. **D98**, 030001 (2018).
[3] A. L. Kagan, Phys. Lett. B **601**, 151 (2004), arXiv:hep-ph/0405134.
[4] M. Beneke, J. Rohrer, and D. Yang, Phys. Rev. Lett. **96**, 141801 (2006), arXiv:hep-ph/0512258.
[5] T. Abe *et al.* (Belle-II), arXiv:1011.0352 [physics.ins-det].
[6] K. Akai, K. Furukawa, and H. Koiso (SuperKEKB), Nucl. Instrum. Meth. **A907**, 188 (2018), arXiv:1809.01958 [physics.acc-ph].
[7] A. J. Bevan *et al.* (BaBar, Belle), Eur. Phys. J. **C74**, 3026 (2014), arXiv:1406.6311 [hep-ex].
[8] B. Aubert *et al.* (BaBar), Phys. Rev. Lett. **95**, 042001 (2005), arXiv:hep-ex/0504001.
[9] G. C. Fox and S. Wolfram, Phys. Rev. Lett. **41**, 1581 (1978).
[10] J. Lees *et al.* (BaBar), Phys. Rev. D **85**, 112010 (2012), arXiv:1201.5897 [hep-ex].
[11] Y. Nakahama *et al.* (Belle), Phys. Rev. D **82**, 073011 (2010), arXiv:1007.3848 [hep-ex].
[12] S. Agostinelli *et al.* (GEANT4), Nucl.Instrum.Meth. **A506**, 250 (2003).
[13] D. J. Lange, *Proceedings, 7th International Conference on B physics at hadron machines (BEAUTY 2000): Maagan, Israel, September 13-18, 2000*, Nucl. Instrum. Meth. **A462**, 152 (2001).
[14] H. Albrecht *et al.* (ARGUS), Phys. Lett. B **241**, 278 (1990).
[15] T. Feldmann, M. Jung, and T. Mannel, JHEP **08**, 066 (2008), arXiv:0803.3729 [hep-ph].